Bibliographical reference

Application of the Mirror Source Method for Low Frequency Sound Prediction in Rectangular Rooms, Marc Aretz, Pascal Dietrich and Michael Vorländer, Acta Acustica **vol. 100** (Number 2), 2014, pp. 306-319

DOI

https://doi.org/10.3813/AAA.918710

Acta Acustica united with Acustica
Vol. 100 (2014) 306 – 319

DOI 10.3813/AAA.918710

Application of the Mirror Source Method for Low Frequency Sound Prediction in Rectangular Rooms

Marc Aretz, Pascal Dietrich, Michael Vorländer
Institute of Technical Acoustics, RWTH Aachen University, 52066 Aachen, Germany.
mar@akustik.rwth-aachen.de

Summary
The present study investigates the applicability of the mirror source method (MSM) to the prediction of the low-frequency modally dominated part of a room transfer function (RTF) in rectangular rooms with arbitrary, complex-valued boundary conditions on the room walls. It is known that the errors caused by application of the MSM with complex boundaries stem from the fact that the distances of sources, receivers to the boundary are not small compared to the wavelength. Thus, the study is focused on the 'practical' low frequency limit of the MSM. The study is based on the comparison of low frequency RTFs obtained from the mirror source and the finite element method (FEM), where the FEM results are considered as the reference. In order to allow the mirror source calculation up to very high orders, the study uses an efficient mirror source modeling algorithm for rectangular rooms which allows the assignment of individual frequency and angle dependent complex reflection factors to each of the six walls in the room. The simulation study focusses on four major aspects: (a) The quantification of the errors that are introduced by the mirror source approximation in the case of non-ideally rigid or soft walls as a function of frequency and average absorption in the room; (b) the simulation error due to the truncation of the MS calculation based on two different interrupt criteria (fraction of reverberation time and attenuation of mirror sources); (c) The impact of commonly applied simplifications of representations of the boundary conditions in the MSM (e.g. negligence of angle dependence of the reflection factor, negligence of the phase of the reflection factor) and (d) the influence of the proportions of the rectangular rooms. The presented results show that for moderately damped rectangular rooms of variable proportions the MSM provides a good approximation of the sound field already with reasonable reflection orders, if frequency and angle-dependent complex reflection factors are applied. The errors in narrow bands are typically below 1 dB in the frequency range above roughly once or the twice the Schroeder frequency but an increasing error in flat and long rooms is observed.
PACS no. 43.20.Dk, 43.20.El, 43.55.-n, 43.55.Br, 43.55.Dt, 43.55.Fw, 43.55.Ka

1. Introduction

State-of-the-art room acoustic simulation tools nowadays use hybrid algorithms which combine the mirror source method[1] for the prediction of the early deterministic part of a room impulse response (RIR) with a stochastic ray tracing method (RTM) for the late stochastic part of the RIR [1, 2, 3].

While the RTM is generally based on energetic quantities as sound field descriptors and can thus only capture frequency band averaged energy envelopes of an RIR, the MSM is capable of generating a deterministic room response in time and frequency domain, by accounting for the temporal fine structure of the various sound reflections and thus also the corresponding interference effects. Taking into account that the MSM is originally based on the exact solution of the wave equation for a single sound reflection at an undamped, infinite planar boundary and considering further that Allen and Berkley [4] were able to show that for an undamped rectangular room[2] the MSM converges to the exact solution of the wave equation, it is interesting to investigate and quantify the errors that are introduced by the MSM for the simulation of damped, more complex shaped rooms.

So-called hybrid methods may also involve deterministic ray tracing, beam tracing, or similar algorithms. It should be noted that these methods are inherently mirror source methods as they are based on geometric construction of specular sound paths and on accounting for the reflection and amplitude deterministically.

Received 17 August 2012,
accepted 17 November 2013.

[1] The term *image source* is equally applied in the literature. Throughout this study study we will however use the more illustrative term *mirror source*.

[2] 'Rectangular' room means that the room geometry is a rectangular cuboid.

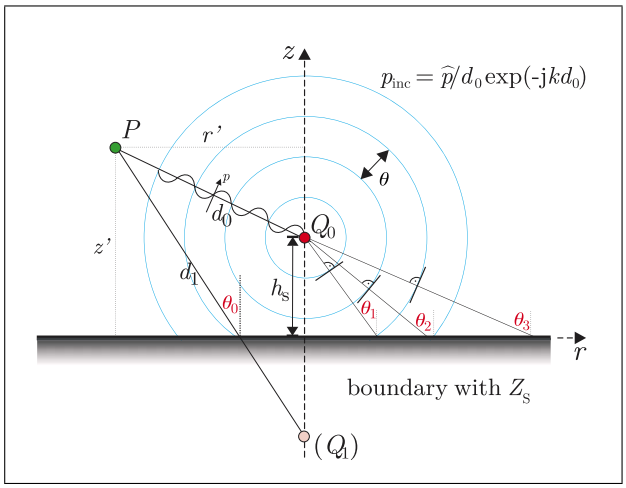

Figure 1. Schematic sketch with coordinate definitions for the reflection of a spherical wave at an extended planar boundary with surface impedance Z_S. Thin blue lines indicate wave fronts.

The present study focuses on the quantification of the accumulated error of MS simulations in damped rectangular rooms and thus extends the considerations by Allen and Berkley [4] to a discussion of the quantitative errors in damped rectangular rooms. The error is assessed by comparison of RTFs obtained from the MS and FE method, where the FE results are considered as the reference.

2. The mirror source method

The mirror source method is based on the principles of geometrical acoustics (GA). According to this theory sound waves are treated much in the same way as light rays are treated in optics. While the principles of GA were already applied in the early days of room acoustics by Eyring [5], Cremer and Müller [6] and first computer implementations of the MSM in rectangular rooms emerged in the early seventies [7, 8, 9], the establishment of the MSM in room acoustic simulation is often associated with the landmark paper by Allen and Berkley [4]. The authors were the first to show that for the special case of a rigid rectangular room the mirror source method yields an equivalent result to the solution of the Helmholtz equation. Finally, in 1984, Borish [10] extended the MSM to arbitrary polyhedra, which however introduced errors due to the negligence of diffraction effects near the edges of the visibility areas of the mirror sources. An extension of the MSM for the consideration of edge diffraction was first presented by Svensson *et al.* [11]. An implementation of this method is realized in the hybrid room acoustic simulation software *RAVEN* [1]. However, the high computational complexity of the method currently limits the applicability to first order diffraction and to rooms with moderate geometrical complexity. Extensions to second-order diffraction were discussed by Svensson [12]. An extensive elaboration on the MSM including the consideration of edge diffraction is given by Mechel [13].

2.1. A point source above an extended planar boundary

As mentioned earlier the MSM yields an exact solution to the wave equation for the reflection of a spherical sound wave at an undamped, infinite planar boundary. The present subsection investigates the error of the MSM in the case of an infinite damped locally reacting planar boundary.

In order to describe the reflection of a spherical sound wave above a locally reacting extended planar boundary as a function of the acoustic surface impedance $\underline{Z}_S$ it needs to be considered that for a point source Q_0 at distance h_s to the absorber plane the angle of incidence on the absorber plane gradually changes from perpendicular to grazing the further the considered point on the plane is away from the source. Consequently, different portions of the incident sound wave are reflected differently depending on their angle of incidence on the absorber. This is indicated in Figure 1. To give an exact solution for this setup the incident spherical sound wave can be decomposed into an infinite sum of plane waves [14, p.516ff]. The spherical wave reflection is then calculated by the superposition of the reflected plane waves where the summation has to account for the angle dependence of the reflection factor and the phase shift on the way from the source point over the reflection point to the receiver point for each plane wave contribution. The angle-dependent reflection factor $\underline{R}(\theta_0)$ can be given as a function of the surface impedance $\underline{Z}_S$, the characteristic impedance of air Z_0 and the specular reflection angle θ_0 as:

$$\underline{R}(\theta_0) = \frac{\underline{Z}_S - Z_0/\cos\theta_0}{\underline{Z}_S + Z_0/\cos\theta_0}. \tag{1}$$

Using this approach the resulting sound field for a normalized[3] point source on the z-axis at distance h_s to the absorber plane, which lies perpendicular to the z-axis, can thus be given in cylinder coordinates (r, z) as [14, p.521ff], [15],

$$\underline{p}_{total}(r,z) = \underline{p}_{inc} + \underline{p}_{refl} = \frac{1}{|\boldsymbol{d}_0|} e^{-jk|\boldsymbol{d}_0|} + jk \int_{\Gamma_\theta} J_0(kr' \sin(\underline{\theta})) e^{-jk(z'+h_s)\cos\underline{\theta}} \underline{R}(\underline{\theta}) \sin\underline{\theta}\, d\underline{\theta}, \tag{2}$$

where $\boldsymbol{d}_0$ is the distance vector between the receiver point $P = (r', z')$ and the source point $Q_0 = (0, h_s)$ according to Figure 1, J_0 is the Bessel function of zeroth order and Γ_θ is a suitable integration path for the angles $\underline{\theta}$ in the complex plane. The integration path is chosen such that the integral over the plane wave contributions spans over all possible directions of the propagation vector $\boldsymbol{k} = (k_x, k_y, k_z)$ with $|\boldsymbol{k}| = k$ and $-\infty < k_x, k_y < +\infty$ (the component k_z is then given by $(k^2 - k_x^2 - k_y^2)^{1/2}$). It is important to

[3] 'Normalized' means in this case that the volume velocity $Q(\omega)$ is chosen such that the point source generates a frequency constant pressure amplitude of 1 Pa at a distance of 1 m in the free field.

mention that in this case it is not sufficient to confine oneself to real-valued angles $\underline{\theta}$ and Mechel [14, p.518] suggests a piecewise linear integration path through the points $(0,0) \rightarrow (\pi/2,0) \rightarrow (\pi/2,-\infty)$, where the first vector entry gives the real part of $\underline{\theta}$ and the second entry the imaginary part respectively. Many publications have dealt with the problem of finding a smart integration path Γ_θ to give useful approximations to the integral formula in equation (2). However, this shall not be a concern of this study and the reader is referred to the excellent elaboration and literature review on the topic by Mechel [14, p.522ff]. In the present study the numerical integration method as applied by Suh and Nelson [15] was used to evaluate the integral in equation (2). The method uses the above mentioned integration path according to Mechel [14, p.518] and separates the integral into a definite integral from $\theta = 0$ to $\pi/2$ and an improper integral from $\theta = \pi/2 + \mathrm{j}0$ to $\pi/2 + \mathrm{j}\infty$. As is shown in [15] the improper integral converges except for grazing incidence ($\theta_0 = \pi/2$).

A simple approximation to the exact formulation in equation (2) can be given by modeling the reflected part of the sound field by a so-called mirror source at $z = -h_\mathrm{s}$ as

$$\underline{p}^*_\mathrm{refl} = \underline{R}(\theta_0)\frac{1}{|\boldsymbol{d}_1|}\mathrm{e}^{-\mathrm{j}k|\boldsymbol{d}_1|}, \tag{3}$$

where $\boldsymbol{d}_1$ is the distance vector between the receiver point $P = (r', z')$ and the mirror source point $Q_1 = (0, -h_\mathrm{s})$ and the specular reflection angle θ_0 is the angle between the boundary surface normal and $\boldsymbol{d}_1$ (cf. Figure 1). In this case the reflected wave corresponds to the sound wave generated by an infinitesimal point source with a directivity function $\underline{R}(\theta)$, which accounts for the angle dependency of the reflection factor.

However, except for the ideally rigid ($\underline{Z}_\mathrm{S} \rightarrow \infty \Rightarrow \underline{R}(\theta) = 1$) or soft ($\underline{Z}_\mathrm{S} = 0 \Rightarrow \underline{R}(\theta) = -1$) cases this source model (infinitesimal point source with a non-uniform directivity function $\underline{R}(\theta)$) constitutes a violation of the wave equation, which especially leads to errors in the near field of the source [13]. More precisely, Mechel states that considerable errors are expected if (a) the sum of heights of Q_0 and P over the wall is not large compared to the considered wavelengths, (b) the specular reflection angle θ_0 gets close to grazing incidence or (c) if the reflection factor $\underline{R}(\theta)$ shows a strong angular variation at the considered reflection angle θ_0 [13].

Figure 2 shows a quantitative assessment of this error for a locally reacting boundary, by plotting the percentage error between equations (2) and (3) as a function of the sum of heights of Q_0 and P and θ_0 for three different exemplary surface impedances $\underline{Z}_\mathrm{S}$, which are taken from the paper by Suh and Nelson [15]. The impedances are chosen such that they span a wide range of different absorption levels. The percentage error E is defined as

$$E = \frac{|\underline{p}^*_\mathrm{refl} - \underline{p}_\mathrm{refl}|}{|\underline{p}_\mathrm{refl}|} \cdot 100.$$

The results in the figure corroborate the strong negative correlation between the error and the normalized sum of heights $(z' + h_\mathrm{s})/\lambda$ as indicated by Mechel [13]. Except near grazing incidence errors already fall below 10% ($\approx$ 1 dB) if the normalized sum of heights exceeds 2 to 3 wavelength. It can further be noted, that for moderate angles of incidence the overall error rises with increasing absorption. However, a generally increasing tendency of the errors towards grazing incidence is not observed for all considered surface impedances at the boundary.

It is finally important to mention that a similar quantitative assessment of the error of the mirror source approximation was presented by Suh and Nelson [15]. They plot the error as a continuous function of θ_0 for three different normalized radial distances $\frac{r'}{\lambda}$ and the same three surface impedances $\underline{Z}_\mathrm{S}$ as used in the present paper. However, it is important to note the differences with regard to the independent variables used for the error determination. While Suh and Nelson chose $(\theta_0, r', \underline{Z}_\mathrm{S})$, we choose $(\theta_0, z' + h_\mathrm{s}, \underline{Z}_\mathrm{S})$. With regard to room acoustic considerations we believe that it is more instructive to use the sum of heights $(z' + h_\mathrm{s})$ than the radial distance r'. This can for example be explained by considering that the plots by Suh and Nelson misleadingly imply that the error is always small close to normal sound incidence but this result is based on the fact that for a given constant value of r' the sum of heights gets very large near normal incidence. And it is actually the large sum of heights that makes the error small rather than the angle of incidence as can be seen from Figure 2.

2.2. Extension to room acoustic simulations

The modeling of the reflection of spherical sound waves at a planar boundary by a mirror source as described in the previous section is the basis of the MSM in room acoustic simulation. For a room acoustic mirror source simulation the room boundaries have to be approximated by planar surfaces which can be considered as fragments of extended flat planes. In a next step multiple mirror sources are constructed by mirroring the original sound source at all planes belonging to the boundary surfaces of the room. These sources are called mirror sources of first order. Higher order mirror sources, which represent sound paths over multiple wall reflections can then be constructed by mirroring these sources again and again on all planes that are spanned by the room surfaces.

Besides the inherent error of the MS reflection model when applied to damped, infinite planar boundaries as described in the previous section, further errors of a room acoustic MS simulation can be attributed to the negligence of sound diffraction due to the finite size of the room surfaces and the negligence of surface scattering effects at structured boundaries. It should be mentioned at this point that the diffraction and scattering phenomena represent to sides of the same coin, because scattering effects can equally be considered as small scale diffraction effects. Thus, the difference lies mostly in the considered structural dimensions (relative to the wavelength) and in the

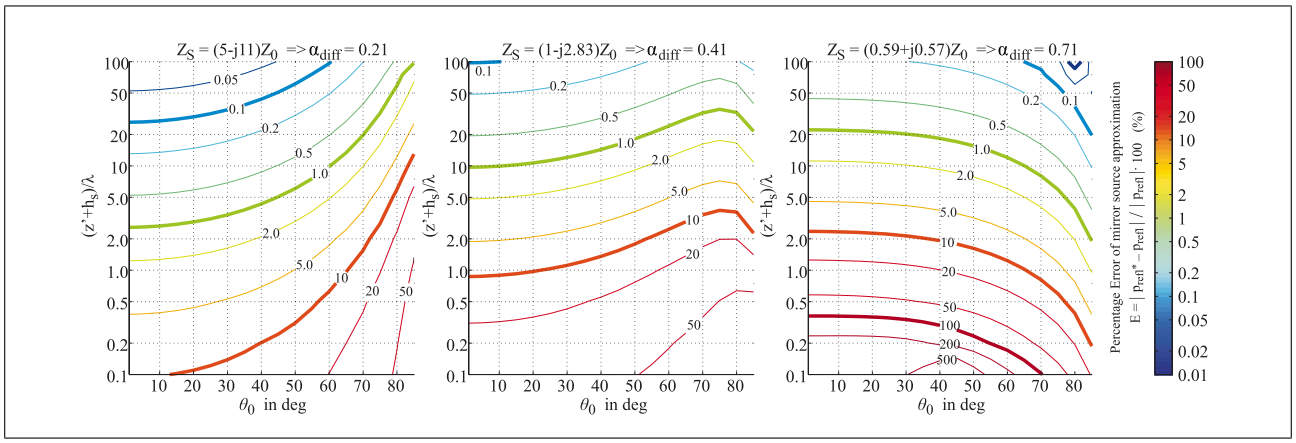

Figure 2. Percentage error of the mirror source approximation (equation: 3) compared to the exact solution (equation: 2). The error is plotted as a function of the normalized sum of heights $(z' + h_s)/\lambda$ and the specular reflection angle θ_0 for three different impedances, which correspond to diffuse field absorption levels of 0.21, 0.41 and 0.71 respectively.

way these phenomena are generally treated in room acoustic simulation software. In the present context the scattering error therefore denotes the error that is introduced by the simplification of a structured surface to a planar boundary, while the diffraction error denotes the negligence of the sound contribution that is bend around a large scale diffraction edge/corner in a room. While the error contributions for the above mentioned phenomena are well elaborated in literature for the case of the sound reflection (diffraction) at a single boundary (edge/corner), only few publications exist, that quantify the accumulated error in a room response in comparison to an exact solution of the wave equation in the considered room. Such an investigation requires a systematic comparison of room modeling with exact representation of multiple edge diffraction versus an approach without diffraction. This problem was in parts discussed by Torres *et al.* [16] and Svensson and Asheim [17].

The rigid rectangular room constitutes an exception in this context. Due to the special symmetry conditions of the rigid rectangular room the diffraction effects—generated at the room corners—cancel each other out and thus a perfect solution of the Hemholtz equation is obtained with the MSM [4]. However, the absence of diffraction effects is a peculiarity of the rigid rectangular room, which can neither be generalized to damped rectangular rooms (if neighboring walls have different impedance characteristics) nor to other room shapes [16].

The present study focuses on the quantification of the accumulated error which is introduced by the MSM in the case of damped rectangular rooms. While part of the error can be attributed to the inherent error of the mirror source approximation (cf. equation (3)) additional errors are introduced by the negligence of the diffraction effects near the edges of the visibility areas of the mirror sources (in the case of inhomogeneous impedances on neighboring room walls and for mirror source orders $n \geq 2$).

It is emphasized that due to the expected increasing influence of diffraction effects in more complex shaped rooms, and the corresponding additional errors in the MS simulations, the results cannot be readily extended to arbitrary room shapes.

3. Implementation details for MSM algorithm

For the present study an optimized *CAFR* (Complex Angle and Frequency dependent Reflection factor) MSM was implemented for the special case of rectangular rooms, which allows the assignment of individual reflection factors $\underline{R}(\theta)$ to each of the six room walls. In order to verify the implemented mirror source algorithm the results were compared to that of Lehmann and Johansson [18][4]. In particular, simulations were run for different real-valued, positive, frequency independent reflection factors on the room walls and a perfect agreement was found[5]. However, it is emphasized that the present CAFR algorithm extends the Lehmann implementation by consideration of complex, frequency and angle-dependent reflection factors.

The impulse response generation consists of three major steps, which are summarized in the following.

3.1. Determination of mirror source positions

In a rectangular room the mirror sources are arranged on a simple regular pattern, which allows the efficient calculation of mirror sources up to very high orders ($n > 50$). A high number of sources is required as the exact solution for the rectangular undamped case is theoretically only

[4] The *MATLAB* based MS implementation by Lehmann and Johansson [18] can be downloaded under http://www.eric-lehmann.com/

[5] In his paper Lehmann suggests the use of negative real-valued reflection factors, which are calculated from given absorption coefficients. This is done to enforce a zero DC offset in the impulse response (IR), since this method results in a negative sign of all mirror source impulses with uneven order in the overall impulse response. However, this method considerably changes the modal structure in the low frequency RTF, since it assumes a 180° phase shift at every boundary. Thus, to compare the results of the present study with that of Lehmann the code by Lehmann was changed to also allow positive real-valued reflection factors.

achieved for an infinitely high number of orders according to [4]. Moreover a visibility test is not necessary in the case of a rectangular room, since each mirror source position on the regular grid corresponds to exactly one visible mirror source. If we assume a rectangular room with dimensions (L_x, L_y, L_z) which has its center at $P_0 = [0, 0, 0]$ and the source and receiver positions at $P_\mathrm{s} = [x_\mathrm{s}, y_\mathrm{s}, z_\mathrm{s}]$ and $P_\mathrm{r} = [x_\mathrm{r}, y_\mathrm{r}, z_\mathrm{r}]$ respectively (see Figure 3) than the position P_MS of a mirror source of order (n_x, n_y, n_z) and its distance $d_\mathrm{MS,r}$ to the receiver are given by

$$d_\mathrm{MS,r}(n_x, n_y, n_z) = \left|\left| P_\mathrm{r} - P_\mathrm{MS}(n_x, n_y, n_z) \right|\right| \quad (4)$$

with

$$P_\mathrm{MS}(n_x, n_y, n_z) = \begin{bmatrix} x_\mathrm{MS} \\ y_\mathrm{MS} \\ z_\mathrm{MS} \end{bmatrix} = \begin{bmatrix} n_x L_x + (-1)^{n_x} \cdot x_\mathrm{s} \\ n_y L_y + (-1)^{n_y} \cdot y_\mathrm{s} \\ n_z L_z + (-1)^{n_z} \cdot z_\mathrm{s} \end{bmatrix} \quad (5)$$

where the order indices $n_{x/y/z}$ are defined as indicated in Figure 3.

3.2. Determination of attenuation of each individual mirror source

In order to calculate the contribution of a single mirror source to the overall room impulse response it has to be considered that each wall reflection can be modeled by a frequency domain multiplication of the excitation spectrum with the complex and angle of incidence dependent reflection factor $\underline{R}(\theta)$. In addition to the sound attenuation at the room boundaries the mirror source contribution also has to be attenuated by $1/d_\mathrm{MS,r}$ to account for the sound decay of a spherical pressure wave propagating in free space. In mathematical notation the attenuation factor A_MS of a mirror source of order (n_x, n_y, n_z) can thus be given as

$$\begin{aligned} A_\mathrm{MS}(n_x, n_y, n_z) = {} & \frac{1}{d_\mathrm{MS,r}} \left(\underline{R}_{\mathrm{x},+} \cdot \underline{R}_{\mathrm{x},-}\right)^{\left\lfloor \frac{|n_x|}{2} \right\rfloor} \quad (6) \\ & \cdot \left(\frac{1 + \mathrm{sign}(n_x)}{2} \underline{R}_{\mathrm{x},+} + \frac{1 - \mathrm{sign}(n_x)}{2} \underline{R}_{\mathrm{x},-} \right)^{(n_x \bmod 2)} \\ & \cdot \left(\underline{R}_{\mathrm{y},+} \cdot \underline{R}_{\mathrm{y},-}\right)^{\left\lfloor \frac{|n_y|}{2} \right\rfloor} \\ & \cdot \left(\frac{1 + \mathrm{sign}(n_y)}{2} \underline{R}_{\mathrm{y},+} + \frac{1 - \mathrm{sign}(n_y)}{2} \underline{R}_{\mathrm{y},-} \right)^{(n_y \bmod 2)} \\ & \cdot \left(\underline{R}_{\mathrm{z},+} \cdot \underline{R}_{\mathrm{z},-}\right)^{\left\lfloor \frac{|n_z|}{2} \right\rfloor} \\ & \cdot \left(\frac{1 + \mathrm{sign}(n_z)}{2} \underline{R}_{\mathrm{z},+} + \frac{1 - \mathrm{sign}(n_z)}{2} \underline{R}_{\mathrm{z},-} \right)^{(n_z \bmod 2)} \end{aligned}$$

where 'mod' is the modulo operator and the complex reflection factors $\underline{R}_{\mathrm{x/y/z},+/-}$, which are assigned to the six room walls according to Figure 3, are of course angle-dependent. The corresponding angles of incidence $\theta_{\mathrm{x/y/z}}$

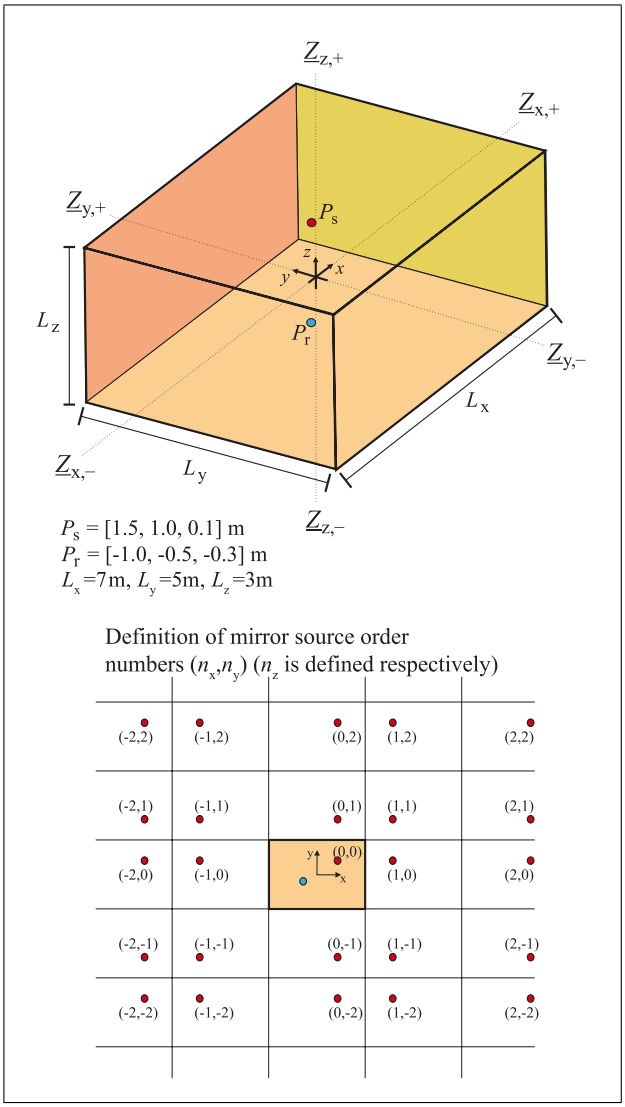

Figure 3. Dimensions, coordinate and variable definition for the rectangular room used for the simulations in sections 5, 6 and 7. The center of the room is positioned at the origin of the coordinate system.

are given by

$$\theta_x(n_x, n_y, n_z) = \arccos\left(\frac{|x_\mathrm{MS} - x_\mathrm{r}|}{d_\mathrm{MS,r}}\right), \quad (7)$$

$$\theta_y(n_x, n_y, n_z) = \arccos\left(\frac{|y_\mathrm{MS} - y_\mathrm{r}|}{d_\mathrm{MS,r}}\right), \quad (8)$$

$$\theta_z(n_x, n_y, n_z) = \arccos\left(\frac{|z_\mathrm{MS} - z_\mathrm{r}|}{d_\mathrm{MS,r}}\right), \quad (9)$$

where θ_x, θ_y and θ_z are the angles of incidence on the walls perpendicular to the x-, y- and z-axis respectively. It is important to mention that in a rectangular room for each individual mirror source only three different angles of incidence exist. This means that for a given mirror source at $P_\mathrm{MS}(n_x, n_y, n_z)$ and receiver point P_r all reflections at the walls perpendicular to the x-axis have the same angle of incidence $\theta_x(n_x, n_y, n_z)$. The same holds for the reflections at the walls perpendicular to the y- and z-axis.

3.3. Calculation of each mirror source contribution to the RIR

With the consideration of frequency dependent reflection factors each mirror source contributes a delayed, attenuated and widened impulse to the overall impulse response. Using the notations from above the room transfer function can be given by the summation of all individual mirror source contributions as

$$\underline{p}_{\mathrm{r}} = \sum_{-n_{\mathrm{x,max}}}^{n_{\mathrm{x,max}}} \sum_{-n_{\mathrm{y,max}}}^{n_{\mathrm{y,max}}} \sum_{-n_{\mathrm{z,max}}}^{n_{\mathrm{z,max}}} \underline{\hat{p}}\, A_{\mathrm{MS}}(n_x, n_y, n_z)\, \mathrm{e}^{\frac{-\mathrm{j}\omega d_{\mathrm{MS,r}}(n_x,n_y,n_z)}{c}}. \quad (10)$$

The room impulse response is then obtained by inverse Fourier transformation. For the implementation of the CAFR mirror source algorithm the given formulas where transferred to a discrete-time and -frequency representation [19].

4. Settings for FE simulations

Throughout this paper all FE simulations were run using the direct frequency domain FEM in *Virtual Lab Revision 10*. The rectangular rooms were meshed with 2nd order tetrahedral elements (10 nodes per element) with an average edge length of 25 cm. Impedance boundary conditions were assigned to the six room walls according to the descriptions in the following sections. The sound source was modeled as a normalized point source, which produces a sound pressure of 1 Pa at 1 m distance in the free field. The source and receiver positions were chosen as indicated in Figures 3 and 11. The simulation frequency range was chosen from 20–450 Hz with a frequency step width of 1 Hz. It is noted that the chosen average edge length satisfies the meshing constraint by Thompson and Pinsky [20] (which requires a minimum of three elements per wavelength for 2nd order elements) throughout the considered frequency range.

5. Verification of *CAFR* MSM algorithm

In a first step MSM and FEM simulations were run for a rectangular room with different complex and frequency dependent surface impedances $\underline{Z}_{\mathrm{S}}$ assigned to the 6 boundaries. In the simulations the room, source and receiver setup of Figure 3 was used. The comparison of the results serves two main purposes: On the one hand the implementation of the MS algorithm shall also be verified in the case of complex-valued, frequency and angle-dependent reflection factors and on the other hand a first assessment of the potential of the MSM to predict the modal structure of an RTF shall be obtained.

In the FE simulation we therefore use the surface impedances as boundary conditions while in the MS simulation we use equation (1) to calculate the angle-dependent reflection factors for each mirror source. Figure 4 shows the normal incidence reflection factors which were calculated from the surface impedances assigned to the room

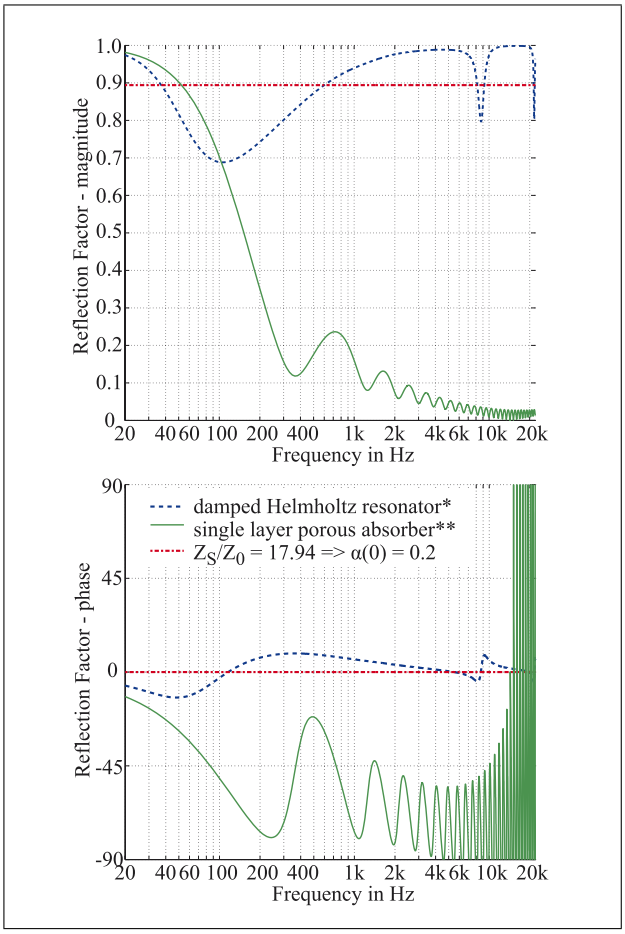

Figure 4. Normal incidence reflection factors $R(0)$ calculated from the surface impedances Z_S that were used in the simulations shown in Figure 5. The complex surface impedances for the single layer porous absorber and the damped Helmholtz resonator were calculated using the two-port network model for layered absorbers described in [21] with the following parameterization. * Damped Helmholtz resonator (3 layers): (1) perforated panel with thickness t = 10 mm, perforation ratio σ_{s} = 0.0314, hole diameter d = 20 mm; (2) flow resistive mass with t = 1 mm, density ρ_{m} = 80 kg/m^3, flow resistivity Ξ = 20 kPa s/m^2; (3) porous absorber layer (Komatsu model [22]) with t = 100 mm, Ξ = 10 kPa s/m^2. ** Single layer porous absorber (1 layer): (1) porous absorber layer (Komatsu model) with t = 200 mm, Ξ = 5 kPa s/m^2.

boundaries. In the case of the two frequency dependent boundary conditions the two-port network model for layered absorbers described in [21] was used to calculate the surface impedances of the heavily damped Helmholtz resonator and the single-layer porous absorber. The corresponding parameterization of the absorber layers is also given in Figure 4.

In order to avoid any artifacts from a too early truncation of the impulse response the truncation time for the MS order has been set to a very conservative value of t_{trunc} = 0.5 s, which exceeds the predicted Eyring reverberation time for the whole audible frequency range. Additionally, it has been verified that a further increase of t_{trunc} does not noticeably change the obtained MSM room trans-

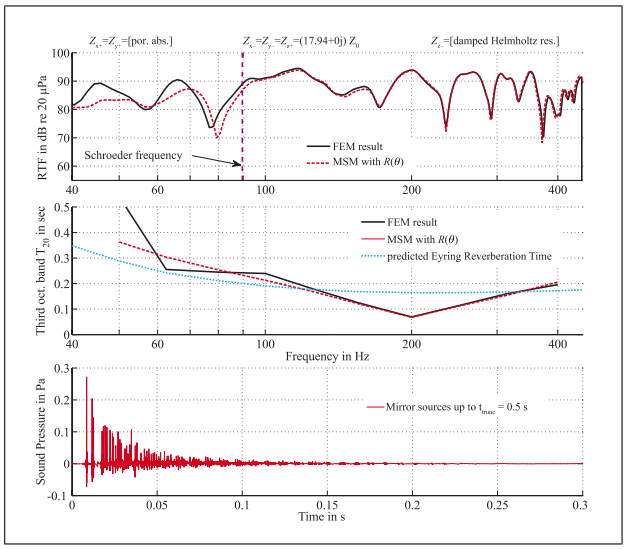

Figure 5. Comparison of low frequency room transfer function and reverberation time in a rectangular room obtained with the FE and MS method for distributed, frequency dependent, complex impedances on the room walls. The bottom plot shows the broadband IR obtained from the MS method. The MS method uses a frequency and angle-dependent reflection factor, which is calculated from the frequency dependent, complex impedances on the six room walls. The reflection factor of the used porous absorber and the damped Helmholtz resonator are given in Figure 4. The normalized impedance on the other three walls ($\zeta = 17.94$) corresponds to an absorption of 0.2 for normal sound incidence.

fer function in the considered frequency range. It can thus be stated that the remaining differences between the FEM and MSM calculation are only caused by the inherent errors of the MSM, i.e. the approximation error of equation (3) and the negligence of diffraction effects at the room boundaries. Figure 5 shows the results of the simulations. It can be seen that in the considered case an excellent match between the transfer functions and reverberation times from both methods is obtained except for frequencies below 100 Hz. Below this frequency the FEM and the MSM results slowly drift apart. However, the dominant dips and peaks caused by the fundamental room modes are still roughly covered by the MSM prediction even down to approximately 50 Hz.

This interesting result agrees well with the general wavelength dependence of the inherent errors of the MSM. Both the error of the mirror source approximation (cf. equation (3) and Figure 2) and the negligence of diffraction yield increasing errors towards lower frequencies [16]. Although, it is not possible to separate the contributions from both sources of error in the simulation results, the results indicate that if complex surface impedance data is available for all room boundaries and the mirror sources can be determined up to sufficiently high orders, the *CAFR* MSM is capable of predicting the modal structure of the low frequency sound field in rectangular rooms with high accuracy, except for the low end of the frequency range. In particul ar the results in Figure 5 suggest that the Schroeder frequency [23], which is also plotted in the graphs, gives a good measure for the lower frequency bound of the validity range of the MS simulation. Although the Schroeder frequency is often referred to in literature as the lower frequency bound for the validity of geometrical acoustics, its deduction is founded on a very different approach than presented in this paper. The Schroeder frequency is based on modal overlap in the frequency domain while the errors of the CAFR MSM are caused by the MS approximation and the diffraction errors at the finite room boundaries. Although all phenomena are related to the relation of room proportions and considered wavelength, a direct link between the validity of the CAFR MSM and the Schroeder frequency would be a surprising result.

The Schroeder frequency will therefore also be plotted in the subsequent sections to investigate if this implication can also be confirmed in rooms with different damping and proportions.

6. Error due to truncation at maximum MS order based on different interrupt criteria

By taking into account the considerable computational complexity of high order mirror source determination in arbitrary rooms, it is now interesting from a practitioners point of view to investigate, up to which mirror source order the results need to be calculated at minimum to get a stable low frequency response and how suitable interrupt criteria can be defined for the MSM.

To approach this question the room setup shown in Figure 3 was used with three different damping configurations ($\alpha_{\mathrm{diff},1} = 0.21$, $\alpha_{\mathrm{diff},2} = 0.41$, $\alpha_{\mathrm{diff},3} = 0.71$) and two different interrupt criteria for the mirror source calculation. The exemplary values of the surface impedances are again taken from the paper by Suh and Nelson [15] to allow comparison between the results.

Firstly, the mirror sources are calculated up to different fractions of the predicted Eyring reverberation time T_{E} and secondly the mirror sources are calculated up to different maximum attenuation factors relative to the direct sound. The attenuation interrupt criterion discards all mirror sources with $10\log_{10}(|e_{\mathrm{MS}}|/|e_{\mathrm{direct}}|) < A$, where e_{direct} and e_{MS} are the energies of the direct sound impulse and the considered mirror source reflection impulse and A is the attenuation threshold in dB. The impulse energies are calculated as the squared sum over all time samples unequal zero. The results for both interrupt criteria are given in Figures 6 and 7 respectively. It can be seen that irrespective of the average room absorption the low frequency room impulse response becomes stable at about $t_{\mathrm{max}} = 0.3\,T_{\mathrm{E}}$ in the case of the first and for $A_{\mathrm{max}} = 40$–50 dB in the case of the second interrupt criterion. It has to be pointed out that both criteria are not equivalent. While the decay of the Schroeder curve at $t_{\mathrm{max}} = 0.3\,T_{\mathrm{E}}$ is approx. $0.3 \times 60\,\mathrm{dB} = 18\,\mathrm{dB}$, the level of single sound reflections (as addressed by the second criterion) arriving around this time are much lower in energy. Thus, along

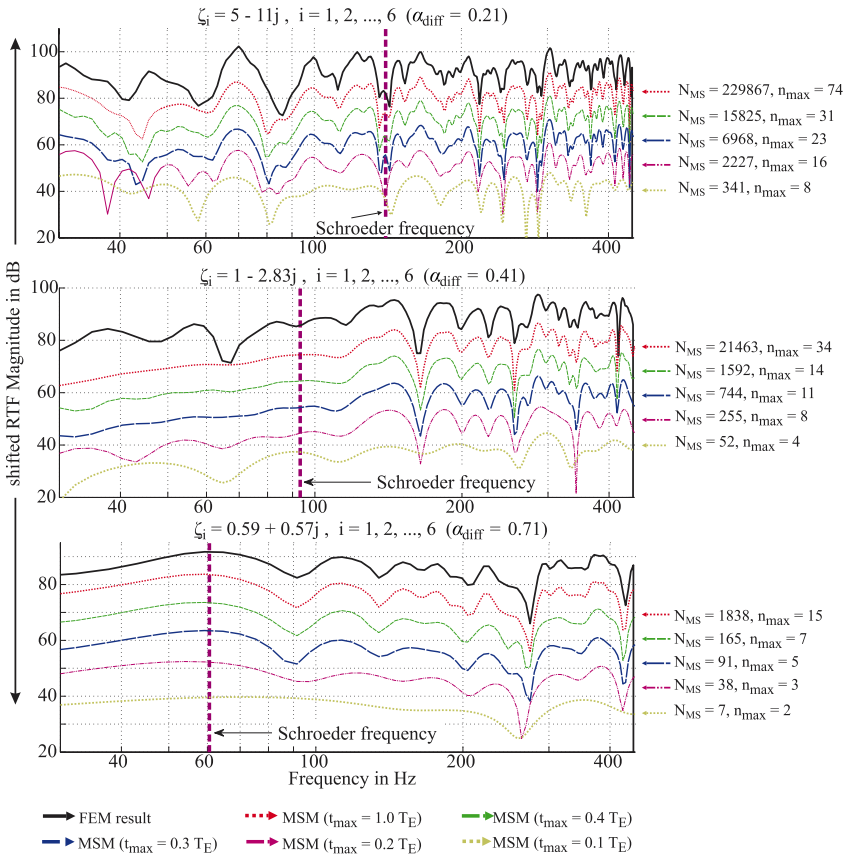

Figure 6. Comparison of low frequency RTF in a rectangular room of 7×5×3 m^3 obtained with FE and MS method for three different average absorption values (RT interrupt criterion). The MS method is calculated up to different truncation times, which correspond to fractions of the predicted Eyring reverberation time. The highest mirror source order n_{max} for each truncation time as well as the total number of considered mirror sources N_{MS} is given in the legend. The RTF magnitudes are shifted by 10 dB for better distinction of the curves.

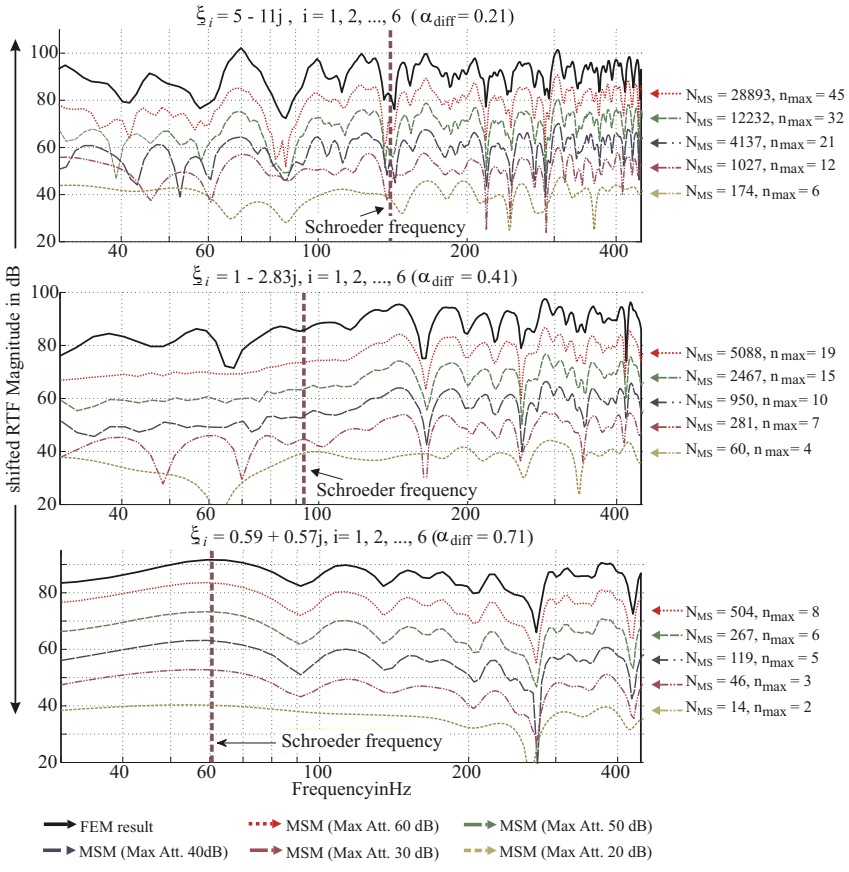

Figure 7. Comparison of low frequency RTF in a rectangular room of 7 × 5 × 3 m^3 obtained with FE and MS method for three different average absorption values (Attenuation interrupt criterion). The MS method only considers mirror source reflections whose magnitude exceed a given threshold level which is given relative to the direct sound level. The MS curves are plotted for 5 different thresholds and the highest order mirror source n_{max} for each threshold as well as the total number of considered mirror sources N_{MS} is given in the legend. The RTF magnitudes are shifted by 10 dB for better distinction of the curves.

with the increasing reflection density over time the discrepancy between the values obtained with criterion 1 and 2 can be explained.

The fundamental modal structure is however already well captured at even smaller values of these interrupt criteria ($t_{\max} = 0.2\,T_E$ and $A_{\max} = 30$–$40\,\mathrm{dB}$). The corresponding highest reflection orders and the total number of necessary mirror sources for these values of the interrupt criteria obviously depend on the average absorption in the room and are also given in Figures 6 and 7.

By looking at the reference MSM results with $t_{\max} = 1.0T_E$ another interesting observation can be made. Firstly, it can be seen that irrespective of the average room absorption the MSM shows a very good match with the FEM results above the Schroeder frequency f_S. However, below f_S the highest deviation is found for an average absorption of $\alpha_{\mathrm{diff}} = 0.41$. Although it was shown in section 2.1 that the error of the mirror source approximation increases with increasing wall absorption and thus the biggest error of the mirror source approximation is expected at $\alpha_{\mathrm{diff}} = 0.71$, this observation can be explained by taking into account that at very high average absorption levels the direct sound (which is modeled without error) becomes more and more dominant in the RIR.

Moreover it is interesting to note that the assignment of a homogeneous surface impedance on all six room walls impedes the generation of sound field discontinuities at the edges of the visibility areas of the mirror sources. Thus, no diffraction effects occur in this case. However, when compared to the errors in Figure 5 for a simulation with inhomogeneously distributed impedance values it is still difficult to exactly quantify the influence of the diffraction errors. This is due to the strong influence of the chosen impedance values (and the corresponding damping) on the error in the simulations.

Summing up, it can be concluded that the MSM already gives a good representation of the low frequency sound field at reasonable mirror source orders except for very low frequencies (inherent MS error) and for very low average room absorption (high orders needed). Above the Schroeder frequency FEM and MSM simulation show a very good match with errors rarely exceeding 1 dB. In the considered cases with low ($\alpha_{\mathrm{diff}} = 0.21$) and high ($\alpha_{\mathrm{diff}} = 0.71$) absorption the fundamental modal structure of the sound field is still well captured by the ISM even at frequencies considerably below the Schroeder frequency.

7. Impact of commonly applied modifications to the MSM method

State-of-the-art hybrid geometrical acoustics tools often use modified versions of the above presented *CAFR* mirror source method. These modifications generally concern the used sound field descriptor (complex sound pressure vs. pressure magnitude or energetic quantities) and the definition of the acoustic boundary conditions (absorption coefficient vs. complex reflection factor; angle-dependent vs. diffuse field averaged quantities). The present section investigates the impact of these commonly found modifications on the modal prediction quality of the MSM. In particular, the following aspects are investigated:

1. The use of angle dependent reflection factors vs. the use of incidence-angle averaged reflection factors.
2. The impact of the negligence of the reflection factor phase.

Two simulation sets were run using again the room setup shown in Figure 3 with a homogeneous and frequency constant surface impedance assigned to all 6 room walls in the FEM simulations. For the first simulation set we use $Z_{S,I} = \zeta_{S,I}\ Z_0 = 17.94\ Z_0$ and for the second set $\underline{Z}_{S,II} = (1+4\mathrm{j})\,Z_0$, respectively. Both impedances yield an absorption coefficient for normal incidence of $\alpha(0) = 0.2$. Thus the first impedance can be calculated from the second by setting the phase of the reflection factor $\underline{R}_{II}(0)$ to zero.

Figure 8 shows the results obtained by using the real-valued impedance $Z_{S,I}$ as a reference in the FEM simulations. The MSM results are calculated for different representations of the boundary characteristics, which are described in the following:

- **Full CAFR method**: The reflection factors in the attenuation function for each mirror source (equation 6) are calculated with equation (1) and the angles of incidence are calculated by using equation (7).
- α_{diff} **method**: An angle independent reflection factor $R_{\mathrm{diff}} = \sqrt{1-\alpha_{\mathrm{diff}}}$ is applied in equation (6). The diffuse field absorption coefficient α_{diff} can be calculated from Z_S by using the following formula (c.f. [24, p.15]):

$$\alpha_{\mathrm{diff}} = 8\frac{\zeta_r}{\left(\zeta_r^2+\zeta_i^2\right)^2}\Big(\left(\zeta_r^2+\zeta_i^2\right) - \zeta_r\cdot\ln(1+2\zeta_r+\zeta_r^2+\zeta_i^2)\Big) + 8\frac{\zeta_r}{\left(\zeta_r^2+\zeta_i^2\right)\zeta_i}\cdot\arctan\left(\frac{\zeta_i}{1+\zeta_r}\right), \tag{11}$$

$$\text{with}\quad \zeta_r = \Re(\zeta)\quad\text{and}\quad \zeta_i = \Im(\zeta). \tag{12}$$

  For $\zeta_{S,I} = 17.94$ we let the imaginary part of the characteristic impedance tend to zero in the equation. The calculation of α_{diff} is based on the assumption that the sound intensity at the considered boundary is homogeneously distributed over all angles of incidence from 0 to $\pi/2$.
- $R_{\theta=0}$ **method**: Finally we have used an angle independent reflection factor $R_{\theta=0} =$ in equation (6). This means that the reflection factor is always calculated for normal sound incidence, no matter what the actual angle of incidence on the considered boundary.

It can be seen, that except for the simulation with angle-independent reflection factor $\underline{R}(0)$, which shows a considerable overestimation of the reverberation time in the room, all other MSM simulations generally agree well with the FEM results, especially with regard to the modal characteristics of the RTF. The best match is found as

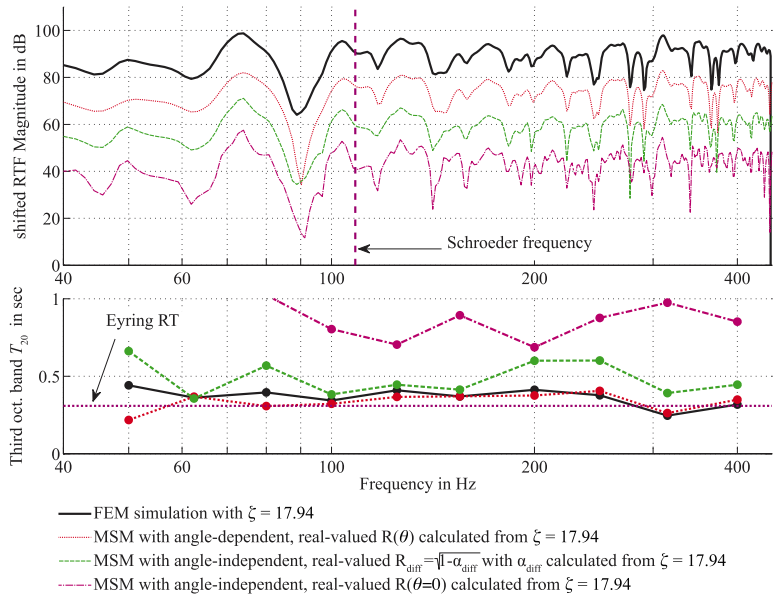

Figure 8. Comparison of low frequency room transfer function and reverberation time in a rectangular room obtained with FE and MS method for a homogeneous, frequency constant and real-valued impedance on all room walls. The MS method uses different boundary representations (see legend). The magnitude of the differently obtained RTFs are shifted by 15 dB for better distinction of the curves.

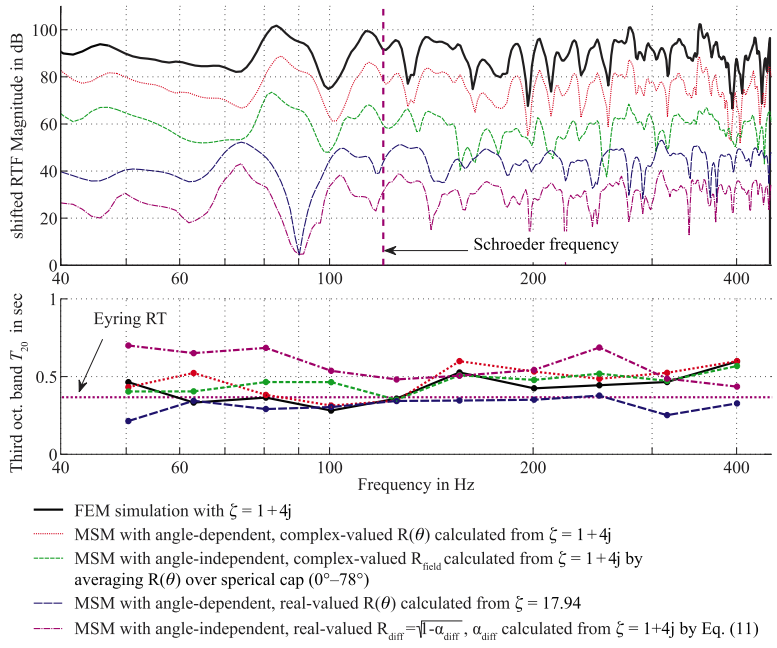

Figure 9. Comparison of low frequency room transfer function and reverberation time in a rectangular room obtained with FE and MS method for a homogeneous, frequency constant and complex impedance on all room walls. The MS method uses different boundary representations. The magnitude of the differently obtained RTFs are shifted by 15 dB for better distinction of the curves.

expected for the full *CAFR* method, but the simulations with the angle-independent diffuse field reflection factor $R_{\mathrm{diff}} = \sqrt{1-\alpha_{\mathrm{diff}}}$ also predict the modal characteristics of the room very well, although the reverberation time is overestimated for frequencies above 160 Hz.

The results using the complex surface impedance $\underline{Z}_{\mathrm{S,II}} = (1 + 4\mathrm{j})\, Z_0$ in the FEM simulations are shown in Figure 9. Again, the MSM simulations were run with different representations of the boundary characteristics. In addition to the full CAFR method (red line), which again yields a very good match with the FE results, further boundary representations have been applied with the focus on the influence of the negligence of the complex character of the reflection factor, its angle dependence or both. Firstly, an MSM simulation was run that uses an angle-averaged complex reflection factor (green line), which shall be denoted 'field incidence reflection factor' $\underline{R}_{\mathrm{field}}$ and which is calculated by averaging the angle-dependent values of $\underline{R}(\theta)$ over a spherical cap from $\theta = 0° - 78°$[6]. This sim-

[6] The field incidence reflection factor is calculated as

$$\underline{R}_{\mathrm{field}} = \frac{\int_{0°}^{78°} \underline{R}(\theta)\sin(\theta)\,\mathrm{d}\theta}{\int_{0°}^{78°} \sin(\theta)\,\mathrm{d}\theta}, \qquad (13)$$

Since ideally diffuse conditions can generally not be obtained in typical rooms, the term 'field incidence' has emerged and is often referred to

ulation preserves the complex character of the reflection factor but applies an averaging over the angles of incidence. It can be seen that the results using this complex-valued field incidence reflection factor roughly reflect the modal structure of the FEM simulation, but the results do not reach the quality of the *CAFR* simulation. Secondly, a simulation was run which neglects the complex character of the boundary characteristics[7] (blue line) by setting the reflection factor phase to zero but accounts for the angle dependency. Finally, a simulation with a real-valued R_{diff} calculated from α_{diff} (purple line, cf. equation 11) was conducted. This boundary characterization corresponds to a negligence of both the complex character as well as an angle averaging of the reflection factor and constitutes the most common method in state-of-the-art room acoustic simulation tools. It becomes evident that both simulations using the real-valued reflection characteristics (blue and purple line) fail to adequately reproduce the modal structure of the RTF throughout the considered frequency range.

Summing up the results in Figures 8 and 9 it becomes clear that it is mostly the negligence of the complex character of the impedance that causes the errors in the modal structure of the sound field and not so much the averaging of the reflection characteristics over all angles of incidence. As mentioned earlier the negligence of the reflection factor phase is one of the most common simplifications of the MSM. This is due to the fact that in most cases only absorption coefficients are known for the boundary materials. Thus, in practical applications a prediction of the modal characteristics of the RTF by using the MSM is often impeded by the lack of appropriate boundary conditions. If complex valued boundary data exists a reliable prediction of the modal characteristics of the RTF appears possible with the MSM above a certain lower frequency bound (at least in the considered rectangular rooms). While this lower freque ncy bound is generally dependent on the source and receiver distance from the considered boundaries, the room proportions as well as the distribution and value of the reflection characteristics on the boundaries, the presented results imply that the Schroeder frequency can be used as a reasonable rough measure for this lower frequency bound.

8. Application to disproportionate rectangular rooms

Acoustically relevant small spaces which may be subject to room acoustic planning and simulation are manifold and include very different shapes and room proportions. These rooms include studio rooms, rehearsal spaces, reverberation rooms, open plan offices, restaurant rooms, passenger cabins in cars, trains or aircraft. While the exact room geometries are generally much more complex than the simple rectangular shape investigated in this study, a first simplified categorization of room shapes can nonetheless be made on the basis of the following three room types: standard rooms (L,W,H in a similar range), flat rooms (L,W $\gg$ H) or long rooms (L $\gg$ W,H). To extend the considerations from the previous sections to all three different room types, comparative simulations have been conducted for three exemplary rooms (one of each type). It is of specific interest whether or not the Schroeder frequency delivers a robust lower frequency limit for the applicability of the image source method. With regard to the boundary conditions reasonable realistic material configurations were chosen and the frequency dependent acoustic surface impedances were again calculated using the layered absorber model described in [21]. For better comparability the boundary conditions were chosen identical in all three rooms. In particular, we assumed an exemplary acoustic ceiling ($\underline{Z}_{\mathrm{z},+}$), a carpet covered lightweight floor ($\underline{Z}_{\mathrm{z},-}$), plate resonators on two side walls ($\underline{Z}_{\mathrm{y},+}$, $\underline{Z}_{\mathrm{y},-}$) and a real-valued frequency constant impedance, which corresponds to a normal incidence absorption coefficient of 0.2 on the other two side walls ($\underline{Z}_{\mathrm{x},+}$, $\underline{Z}_{\mathrm{x},-}$). The resulting absorption properties of the chosen material configurations are given in Figure 10 with a detailed description of the exact layering and parameterization of each absorber.

Figure 11 shows a comparison of the FE and MS simulations obtained in all three rooms, where the truncation time of the MS simulation was set sufficiently high to ensure a stable MS RTF. Additionally the Schroeder frequency is indicated in the graphs for each room. It can be seen, that around and above the Schroeder frequency the MS approximation gives a good fit with the reference FE results for all three rooms. However, below the Schroeder frequency the simulation accuracy degrades noticeably especially for the more disproportionate rooms (long room and flat room). This result is again in good agreement with the error plot shown in Figure 2 for a single mirror source reflection. Based on the results from this plot, the increased simulation error can thus be attributed to the increased contribution from very close reflections and the overall increased angles of incidence in the disproportionate rooms. With regard to the interrupt criteria defined in section 6, it is important to mention that the application of the reverberation time interrupt criterion appears not reasonable in these non-diffuse disproportionate spaces. However, the dB interrupt criterion is still applicable to limit the number of necessary mirror sources even in these spaces.

Finally, Figure 12 assesses the simulation error in the three rooms on a frequency scale which is normalized to the respective Schroeder frequency in each room. In this context the simulation error is defined as the deviation of the sound pressure levels (L_{MS}, L_{FE}) from the MS and FE

in building acoustics (e.g. [25, p. 426ff]). Field incidence assumes that angles of incidence are restricted to being equally probable between 0°-78°. Hopkins states that the upper boundary for the angles of incidence is mostly empirically motivated and somehow lacks a physical meaning [25]. However, the value of 78° has been adopted in many publications because of its commonly observed good fit with measured data.

[7] Setting the reflection factor phase of $\underline{R}(\theta = 0)$ to zero, corresponds to a real-valued characteristic impedance of $\zeta = 17.94$. The blue curve in Figure 9 is thus equivalent to the red curve in Figure 8.

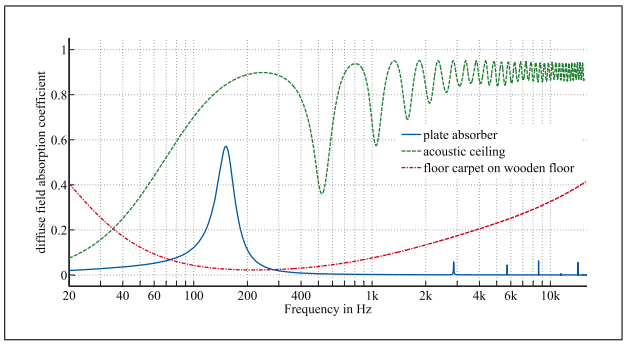

Figure 10. Diffuse field absorption coefficients α_{diff} calculated from the surface impedances $\underline{Z}_{\mathrm{S}}$ that were used in the simulations shown in Figure 11. In order to use realistic, representative boundary conditions for the considered simulation rooms, the two-port network model for layered absorbers described in [21] was used to calculate the surface impedances of an exemplary acoustic ceiling, a damped plate absorber and a thin wooden floor with a carpet covering. The layered absorbers were parameterized as follows: Acoustic ceiling (2 layers, rigid backing): (1) porous absorber layer (Komatsu model [22]) with $t = 50\,\mathrm{mm}$, $\Xi = 10\,\mathrm{kPa\,s/m^2}$; (2) air-gap with $t = 300\,\mathrm{mm}$. Plate absorber (2 layers, rigid backing): (1) surface mass with $t = 5\,\mathrm{mm}$, $\rho_{\mathrm{m}} = 500\,\mathrm{kg/m^3}$ and loss factor $\eta = 0.01$; (2) porous absorber layer (Komatsu model [22]) with $t = 60\,\mathrm{mm}$, $\Xi = 0.2\,\mathrm{kPa\,s/m^2}$. Floor carpet on wooden floor (2 layers, free field termination): (1) porous absorber layer (Komatsu model [22]) with $t = 5\,\mathrm{mm}$, $\Xi = 20\,\mathrm{kPa\,s/m^2}$; (2) surface mass with $t = 20\,\mathrm{mm}$, $\rho_{\mathrm{m}} = 500\,\mathrm{kg/m^3}$ and loss factor $\eta = 0.01$.

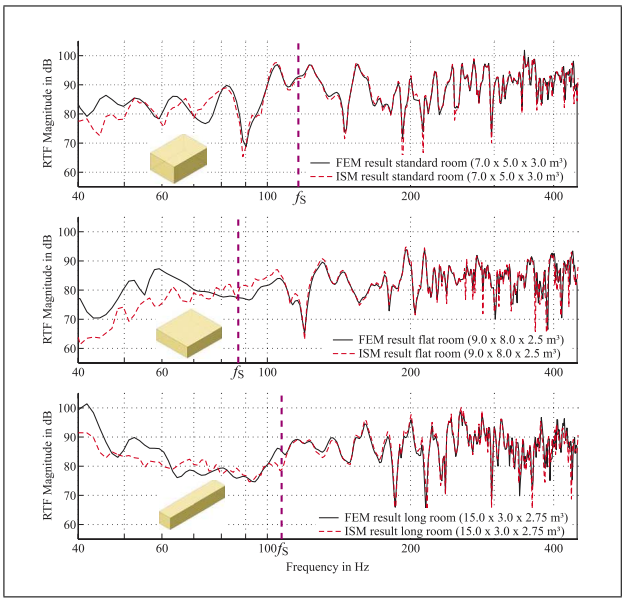

Figure 11. Comparison of low frequency room transfer functions simulated with the FE and the CAFR MSM in three rectangular rooms of different proportions. The boundary conditions were chosen identical for all three rooms according to the descriptions in the text and Figure 10. The source and receiver positions were chosen as follows: Standard room: $P_S = (1500,\ 1000,\ 100)\,\mathrm{mm}$, $P_R = (-1000,\ -500,\ -300)\,\mathrm{mm}$; Flat room: $P_S = (-1800,\ -1300,\ 500)\,\mathrm{mm}$, $P_R = (2700,\ 2100,\ -50)\,\mathrm{mm}$; Long room: $P_S = (-4100,\ -200,\ 375)\,\mathrm{mm}$, $P_R = (2700,\ 100,\ -175)\,\mathrm{mm}$.

simulations (i.e. $\mathrm{Error_{dB}} = L_{\mathrm{MS}} - L_{\mathrm{FE}}$). In addition to error values at every frequency bin, the figure also shows band averaged error values[8]. While the overall error of course also depends on the chosen boundary conditions, the plot gives a reasonable assessment of the applicable frequency ranges of the MSM for the different room types.

In order to interpret the results of this figure the frequency range can be divided into three characteristic regions, i.e. considerably below, around and considerably above the Schroeder frequency (these regions are indicated by the different background color shading in Figure 12). With regard to the latter frequency range it can be stated that despite the fact that the error function shows strong fluctuations above roughly two times the Schroeder frequency, the band averaged error is mostly below ±1 dB in this frequency range. Taking also into account the RTFs shown in Figure 11 it becomes clear that in this frequency range the overall fit between FE and MS simulation is generally very high. The strong error fluctuations thus mostly stem from slight frequency misalignments in the very sharp dips and peaks in the simulated RTFs. In the frequency range around the Schroeder frequency the error generally increases. However, while the standard room and the long room show a very low average error down to approximately $0.8 f_{\mathrm{S}}$ the flat room already shows considerably increased errors already from $1.5 f_{\mathrm{S}}$ downward.

At frequencies far below f_{S} the error increases further for all three rooms, where the flat room continues to show the highest error. In this context it is important to note, that the flat room with a room height of only 2.5 m and the chosen source and receiver position (cf. annotations of Figure 11) has the smallest sum of heights with regard to the close and strongly absorptive ceiling reflection. Thus, the increased error in the flat room simulation again corresponds well to the error plot in Figure 2 for a single mirror source reflection and it can be concluded that in a strict sense the error of the MSM generally depends on the room geometry, the boundary conditions and the chosen source and receiver position in the room. However, our results imply that even in strongly damped rooms with reasonable room proportions and source and receiver positions at a certain distance to the room boundaries[9], the error of the MSM is generally in a range of ±1 dB for frequencies above the Schroeder frequency. On the other hand, it is emphasized again, that any kind of scattering or diffracting objects as generally found in real rooms or a non-rectangular room geometry further increases the error in the MSM simulation. The given error bounds therefore have to be regarded as best case scenarios for idealized rooms.

[8] The band averaged error values are calculated as the root of the arithmetic mean of the square of the ratio $p_{\mathrm{MS}}/p_{\mathrm{FE}}$ in third octave bands. The frequency range for the averaging was set to ±2 octaves around the respective Schroeder frequency of the considered room.

[9] See discussion on the role of the sum of heights $(z' + h_{\mathrm{s}})$ above an absorber plane in section 2.1.

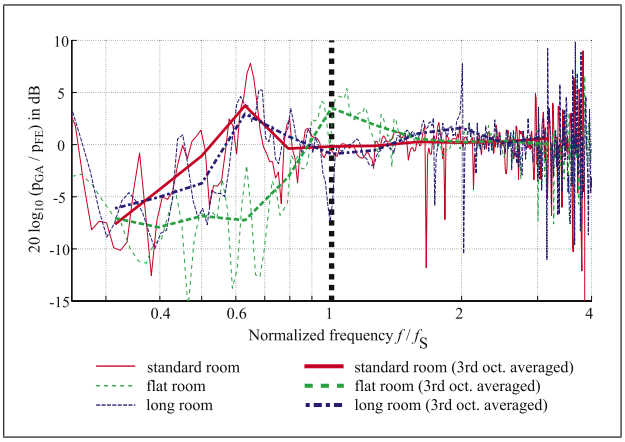

Figure 12. Error in dB of MS simulation for three different rectangular rooms when compared to FE simulation on a normalized frequency axis. The deviation is calculated as $E_{\mathrm{dB}} = L_{\mathrm{MS}} - L_{\mathrm{FE}}$, where L_{MS} and L_{FE} are the sound pressure levels obtained in the MS and FE simulations respectively. The normalization of the frequency axis is conducted by referencing the absolute frequency f in Hz to the respective Schroeder frequency f_{S} for each room.

9. Conclusions

The presented study investigates the applicability of the mirror source method to the prediction of low frequency sound fields in rectangular rooms compared to the wavelength. In particular, it can be stated that, when compared to FE simulations in a damped rectangular room, the error of the CAFR MSM is generally in a range of ±1 dB at frequencies around and above the Schroeder frequency f_{S}. In all cases studied—including the long room—a frequency range of $f > 2f_{\mathrm{S}}$ was shown to be adequate for sufficiently accurate results with errors smaller than 1 dB even in narrow bands.

Moreover, it was confirmed that as expected the prediction of the modal structure of the sound field using the MSM is generally only possible if complex-valued surface impedances are used as boundary input data. Only in the case of rather hard reflecting walls the use of real-valued boundary data is admissible, since in this case the reflection factor phase is close to zero anyway. Additionally, it can be stated that it is always preferable to account for the angle dependence of the reflection factor instead of using diffuse field averaged values, since if the complex surface impedances are known and the boundaries are considered locally reacting (with $\underline{Z}_{\mathrm{S}} \neq f(\theta)$) the inclusion of the angle dependency comes at a low additional computational cost.

Further work should focus on the identification of guidelines for a lower frequency limit depending on the boundary conditions and the room shape. Long and flat rooms showed larger errors, and this is expected to be explained by the ratio of room dimensions rather than by the Schroeder frequency alone. Finally, it has to be kept in mind that the present results are not readily applicable to more general room shapes due to the expected increasing influence of diffraction errors. The influence of these diffraction effects on the modal structure of the sound field therefore needs to addressed. For a more valid conclusion on the influence of the room shape further work is required in order to identify a robust frequency limit below which numerical wave models are unavoidable.

References

[1] D. Schröder: Physically based real-time auralization of interactive virtual environments. Dissertation. Institute of Technical Acoustics, RWTH Aachen University, 2011.

[2] G. Naylor: Odeon - another hybrid room acoustical model. Applied Acoustics **38** (1993) 131–143.

[3] B. Dalenbäck: Engineering principles and techniques in room acoustics prediction. Baltic-Nordic Acoustic Meeting, Norway, 2010.

[4] J. B. Allen, D. A. Berkley: Image method for efficiently simulating small-room acoustics. The Journal of the Acoustical Society of America **65** (1979) 943–950.

[5] C. F. Eyring: Reverberation time in "dead" rooms. The Journal of the Acoustical Society of America **1** (1930) 217–241.

[6] L. Cremer, H. Müller: Principles and applications of room acoustics (translated by t.j. schultz). vol.I & vol. II. Applied Science, London, 1982. Translation with revisions of: Die wissenschaftlichen Grundlagen der Raumakustik. Stuttgart, S. Hirzel, 1948-61.

[7] J. Berman: Behavior of sound in a bounded space. The Journal of the Acoustical Society of America **57** (1975) 1275–1291.

[8] B. Gibbs, D. Jones: A simple image method for calculating the distribution of sound pressure levels within an enclosure. ACUSTICA **26** (1972) 24–32.

[9] F. Santon: Numerical prediction of echograms and of the intelligibility of speech in rooms. The Journal of the Acoustical Society of America **59** (1976) 1399–1405.

[10] J. Borish: Extension of the image model to arbitrary polyhedra. The Journal of the Acoustical Society of America **75** (1984) 1827–1836.

[11] U. P. Svenson, R. I. Fred, J. Vanderkooy: An analytic secondary source model of edge diffraction impulse responses. The Journal of the Acoustical Society of America **106** (1999) 2331–2344.

[12] U. P. Svensson: Modelling scattering with high orders of diffraction. Proceedings of AIA-DAGA, Merano, Italy,, 2013.

[13] F. Mechel: Improved mirror source method in roomacoustics. Journal of Sound and Vibration **256** (2002) 873–940.

[14] F. Mechel: Schallabsorber. Band 1. äussere Schallfelder - Wechselwirkungen. S. Hirzel Verlag, Stuttgart, 1989.

[15] J. S. Suh, P. A. Nelson: Measurement of transient response of rooms and comparison with geometrical acoustic models. The Journal of the Acoustical Society of America **105** (1999) 2304–2317.

[16] R. R. Torres, U. P. Svensson, M. Kleiner: Computation of edge diffraction for more accurate room acoustics auralization. The Journal of the Acoustical Society of America **109** (2001) 600–610.

[17] U. P. Svensson, A. Asheim: Time-domain formulation of an edge source integral equation. The Journal of the Acoustical Society of America **133** (2013) 3491–3491.

[18] E. A. Lehmann, A. M. Johansson: Prediction of energy decay in room impulse responses simulated with an image-

source model. The Journal of the Acoustical Society of America **124** (2008) 269–277.

[19] A. Oppenheim, R. Schafer, J. Buck: Discrete-time signal processing. Prentice Hall, 1999, (Prentice-Hall signal processing series).

[20] L. L. Thompson, P. M. Pinsky: Complex wavenumber fourier analysis of the p-version finite element method. Computational Mechanics **13** (1994) 255–275.

[21] F. Mechel: Schallabsorber. Band 3. Anwendungen. S. Hirzel Verlag, Stuttgart, 1998.

[22] T. Komatsu: Improvement of the Delany-Bazley and Miki models for fibrous sound-absorbing materials. Acoustic Science & Technology **29** (2008) 121–129.

[23] M. Schroeder: Die statistischen Parameter der Frequenzkurven von grossen Räumen. Acustica **4** (1954) 594–600.

[24] F. Mechel: Schallabsorber. Band 2. Innere Schallfelder - Struk turen. S. Hirzel Verlag, Stuttgart, 1995.

[25] C. Hopkins: Sound Insulation. Butterworth-Heinemann, 2007.